An Investigation of Acoustic-to-Seismic Coupling to Detect Buried Antitank Landmines

James M. Sabatier and Ning Xiang

***Abstract*—When an acoustic wave strikes the ground surface, energy is coupled into the motion of the fluid/solid frame comprising the ground. This phenomenon is termed acoustic-to-seismic (A/S) coupling. In the ground, the Biot Type II or Biot slow waves travel with a speed well below the speed of sound in air. The porous nature of the ground causes the entering acoustic wave to bend toward the normal and the acoustic wave propagates downward into the ground. When an object is buried a few cm below the ground surface, it distinctly changes the A/S coupled motion. These changes can be sensed by measuring vibrational particle velocity on the ground surface. Taking advantage of a noncontact remote measurement technique, the A/S coupling measurements for antitank landmine detection are conducted using a laser Doppler-vibrometer (LDV). Recent field measurements in both calibration and blind mine lanes and the resulting data analyses, which demonstrate the effectiveness of this technique, are described in this paper.**

***Index Terms*—Acoustic landmine detection, acoustic-to-seismic (A/S) coupling, laser Doppler vibrometer-based landmine detection.**

I. Introduction

WHEN an airborne acoustic wave is incident at the ground surface, acoustic energy is coupled into the ground as seismic motion. This phenomenon is well-documented and is termed acoustic-to-seismic (A/S) coupling in the relevant literature [1]–[5]. During the early 1980s, the phenomenon of A/S coupling was used to detect buried objects or landmines. In these early measurements, geophones measured the normal component of the ground particle velocity over buried targets. A review of early experimental investigations on A/S coupling for landmine detection can be found in [6]. Recognizing the need for a noncontact sensor and to investigate the geophone/soil coupling effect on the A/S transfer function, a feasibility study using a laser Doppler vibrometer (LDV) was conducted in early 1990s [7]. Following the success of this study, additional measurements were made on buried mines or mine-like objects using the LDV. These studies paved a new road toward developing a LDV-based acoustic mine detection system [6]. With the advancing development of LDV technology, more recent field measurements have been conducted using a scanning LDV [8]. The capability of the LDV-based acoustic landmine detection system developed by the University of Mississippi has been tested at the University of Mississippi and U.S. Army test sites.

In this paper, the underlying physics of A/S coupling pertaining to landmine detection is reviewed briefly in Section II. Section III emphasizes A/S coupling measurements using a noncontact, remote sensor: a scanning LDV. Section IV describes recent blind field testing at U.S. Army test sites and discusses the major results achieved during that field testing.

II. Review of the Underlying Physics

When airborne sound is incident on the surface of a soil, air contained by connected pores in the soil is caused to oscillate in and out of the pores. The resulting area-average volume flow is governed both by the frequency and amplitude of the sound waves and by the properties of the soil. The energy from the vibrating air above the soil surface couples with the air in the soil pores. Hence, the penetration of the sound waves is strong if the air permeability is high. The transmitted sound is attenuated by viscous friction present at the pore walls. Conversely, low air permeability results in weak coupling and little sound penetration. Through momentum transfer at the air–soil boundary and viscous attenuation at the pore walls, the energy is transferred to the soil frame. Strictly speaking, this transfer of energy to the fluid-filled soil must be treated using a poro-elastic wave theory. Biot's model has been used to successfully describe this coupling [3].

The Biot equations of motion include two compressional wave solutions and thus two propagation constants or wave speeds. The waves are referred to as the waves of the first and second kinds or simply as "fast" and "slow" waves. Both of these waves propagate simultaneously in both fluids and solids so that there is both fluid and solid displacement for each wave. The fast wave is analogous to the compressional or seismic *p*-wave that propagates in a solid. It is relatively unattenuated and is not dispersive. The slow wave is a diffusion wave that is highly attenuated and very dispersive as it propagates [5]. Experimental studies conducted in Reference [5] show that it is this slow wave that carries most of the transmitted energy into the ground.

The key aspect of the physics of air-filled solids as used in acoustic technology for mine detection is that airborne sound is preferentially coupled into the soil as slow wave energy [1]–[5]. The speed of this wave is much slower than the sound speed in air, so the slow wave is refracted toward the normal. The slow wave dilates both the air and the soil frame as it propagates. Therefore, slow wave effects can be detected by sensing the

Manuscript received June 1, 2000; revised February 21, 2001. This work was supported by the U.S. Army Communications-Electronics Command Night Vision and Electronics Sensors Directorate.

The authors are with the National Center for Physical Acoustics, University of Mississippi, University, MS 38677 USA (e-mail: sabatier@olemiss.edu; nxiang@olemiss.edu).

Publisher Item Identifier S 0196-2892(01)05112-9.

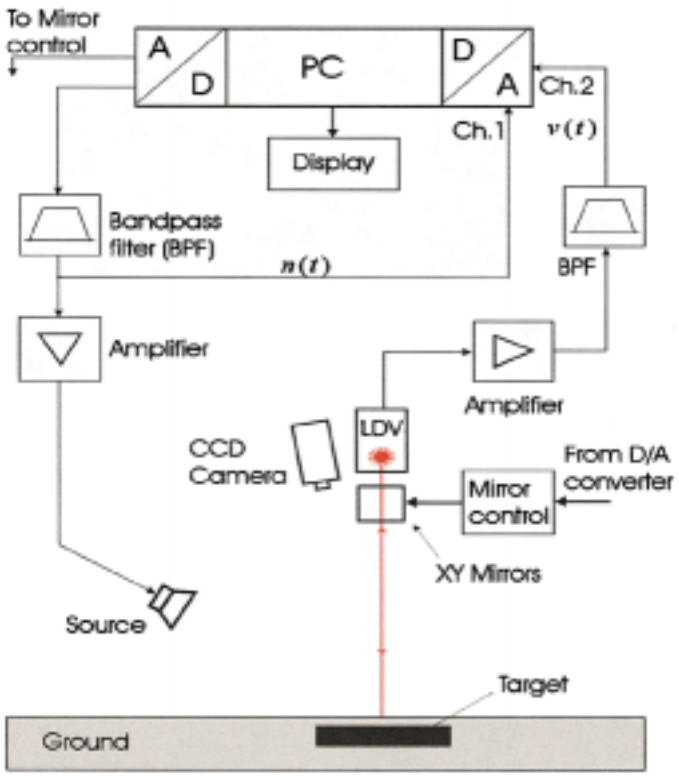

Fig. 1. Setup for A/S landmine detection field measurements using a scanning laser Doppler vibrometer (LDV). $v(t)$ represents a band-pass filtered output voltage from LDV, while $n(t)$ for a band-pass filtered pseudo-random noise driving the sound source.

Fig. 2. Photograph of the LDV-based A/S mine detection system during a field measurement. Two loud speakers were used as a sound source. The LDV unit was mounted onto a vehicle-based platform. The laser beam of the LDV sensed the ground surface in a remote, raster-scanned manner.

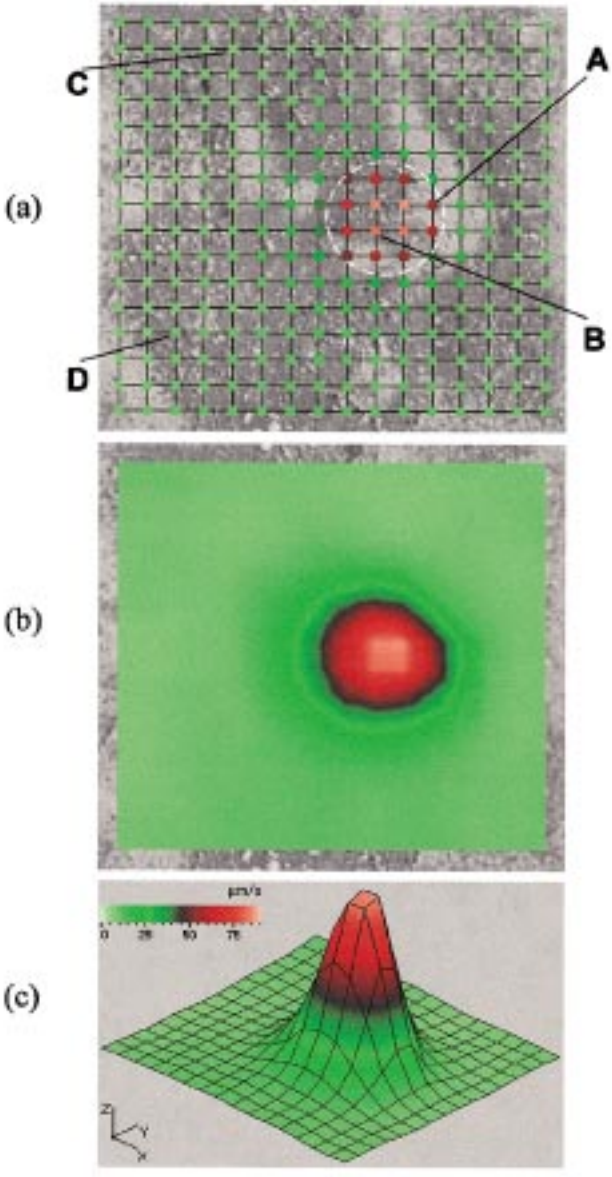

Fig. 3. A grid of 16 × 16 is defined covering a scanned patch of 1 m × 1 m resulting in a spatial resolution of 6.7 cm. It is superimposed on the image of the road surface at U.S. Army Test Lane 11. A VS 2.2 plastic mine is buried 7.5 cm deep. The integrated (RMS) velocity value in a frequency band between 130 Hz and 160 Hz is represented. (a) Color dots. The dot-line circle indicates the target location. Color scale is given in (c). In Fig. 4, individual measured magnitude spectra on points A, B, C, and D are illustrated. (b) Color map, achieved from (a) in terms of interpolation and spatial filtering. Color scale is given in (c). (c) Three-dimensional (3-D) color map derived from (b).

movement of either the frame or the gas. The attenuation of the slow wave is well-modeled and occurs rapidly with depth [5]. It seems highly plausible that the slow wave scatters from targets buried in soils and reflects back to the surface, affecting the vibrational velocity of the surface. Detection depth for buried objects is controlled by the slow wave attenuation coefficient. Target resolution is controlled by the wavelength of the slow wave and spacing of the sensor measurements. Nonporous inhomogeneities are acoustically detected in soils by means of these physical phenomena. Experimental results show that the A/S coupling measurement technique can detect both metallic and nonmetallic landmines.

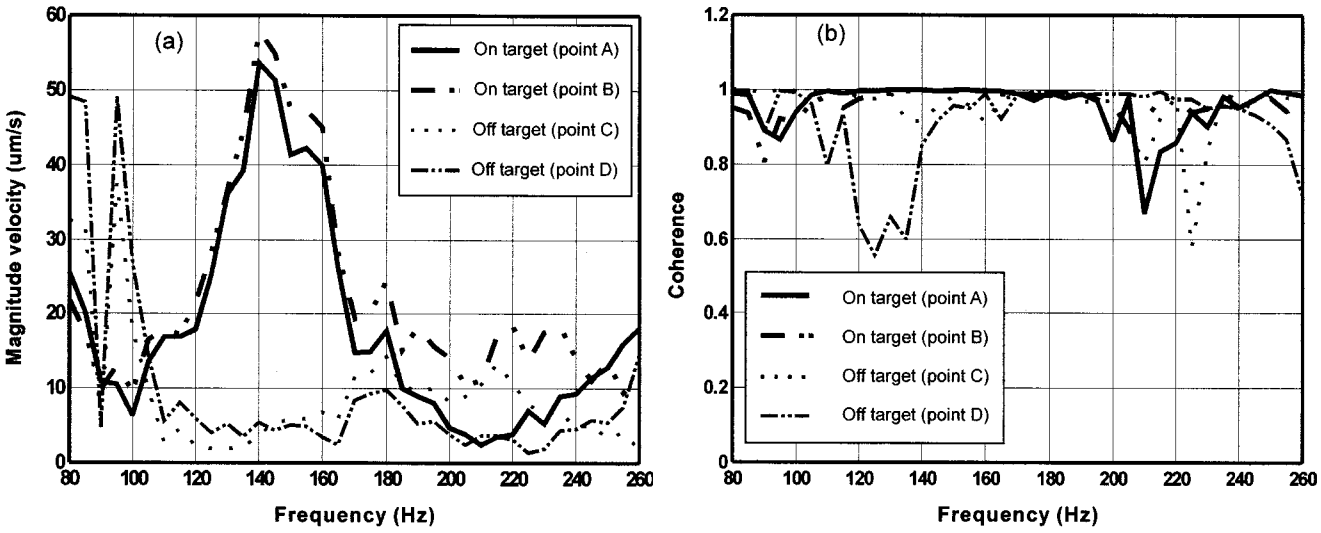

Fig. 4. Measured data on a plastic VS 2.2 anti-tank mine presented as functions of frequency at point A, B, C, and D marked in Fig. 3. (a) Magnitude spectra. (b) Coherence functions.

III. Experimental Measurement of A/S Coupling

A. Laser Doppler Vibrometer

The vibrational velocity on the ground surface is sensed using a laser Doppler vibrometer (LDV). In the current experimental study, a single-point interferometer is employed. A laser beam is emitted from the LDV onto a vibrating surface of an object under test; the surface vibrational velocity causes a Doppler frequency shift of the laser light. The backscattered light from the measured object takes the opposite path back into the interferometer and is sensed by its photo-detector (see [9] for more details about a LDV). As a result, a frequency-modulated (FM) signal from the photo-detector carries the information about the surface velocity. After FM-demodulation of the detector output, the signal is proportional to the surface velocity under test. For the purposes of the present discussion, it is sufficient to mention that the output of a LDV system is a voltage proportional to the instantaneous velocity of a particular spot on the object under test.

B. Acoustic-to-Seismic (A/S) Coupling Measurement Setup

For the detection of anti-tank mines, A/S coupling measurements are performed using a scanning LDV (PSV 200 manufactured Polytec P I, Inc). Fig. 1 schematically illustrates the measurement setup employed in outdoor field measurements. The LDV system is equipped with a video camera and X–Y scanning mirrors. A video image of the ground surface of interest can then be displayed on a PC monitor. A grid of varying sizes consisting of points to be scanned can be defined and superimposed on the image of the ground surface. During scanning, a sound source radiates pseudo-random noise typically covering the frequency range between 80 Hz and 300 Hz. This range was selected based on the results of experiments conducted in the frequency range between 40 Hz and 4 kHz. These experiments revealed the optimal frequency range lies between 100 Hz and 250 Hz for anti-tank landmines buried not deeper than 20 cm (8 inches). On the scanned patch, the sound pressure level can range between 90 dB (C) to 120 dB (C). The angle of sound incidence is not critical since the porous ground is locally reacting [4].

Fig. 2 shows a photograph of the LDV-based A/S landmine detection system used in a recent blind field test. In this test, the LDV unit was placed 3.5 m high above the ground and the laser beam was focused downward onto the surface. Two loudspeakers (Peavey 118 Sub HC) were used as a sound source. They were placed approximately 1 m above the ground and 1.8 m from the center of a scanned patch.

The scanning procedure includes mirror control in a raster scan manner, data collection, and data analysis. In the current measurement setup, the sound source radiates periodic pseudo-random noise and the X–Y mirrors move the laser beam to predefined grid points one after the other. The response to the acoustic periodic excitation is the instantaneous vibrational velocity of the ground surface and, which is collected through a data collection channel, Fourier-transformed, and averaged over several periods in a complex frequency domain. As the result, a complex velocity function $\tilde{V}(f)$ is collected at each grid point. At the same time, a complex function $\tilde{N}(f)$ of periodic pseudo-random noise is also collected through another data collection channel (as shown in Fig. 1).

C. Data Analysis

To image the mine location from the scanning results, the magnitude of the spectrum of the velocity function $\tilde{V}(f)$ at each grid point is integrated over a frequency band chosen because of the occurrence of consistent amplifications in magnitude in the presence of mines

$$M_{ij} \sim \int_{f_1}^{f_2} \left| \tilde{V}_{ij}(f) \right| df. \tag{1}$$

f_1, f_2 denote the lower and upper frequency limits, respectively. i, j are the subscripts of a grid point on the ith row and the

jth column of the grid. In this way, magnitude values can be presented as data points on a color map.

A typical scanning result in form of color (grayscale) dots is shown in Fig. 3(a), in which colors (grayscales) are assigned proportionally to the integrated values of magnitude velocity. This particular result was for a plastic VS 2.2 mine buried 7.5 cm deep in U.S. Army Test Lane 11 at Fort A. P. Hill. The VS 2.2 mine is roughly cylindrical with a top-view diameter of 24 cm. Fig. 3(a) illustrates a 16-points by 16-points grid covering a patch of 1 m $\times$ 1 m. The grid is superimposed onto the video image of the ground surface. A surface velocity function $\tilde{V}(f)$ is evaluated using (1) at each grid point. A frequency resolution of 2.5–10 Hz is often used to represent the discrete velocity function $\tilde{V}(f_i)$. For example, Fig. 4(a) shows the magnitude spectra of velocity functions on and off the target for the same mine.

The coherence function between the sending pseudo-random noise $\tilde{N}(f_i)$ and the velocity function $\tilde{V}(f_i)$ at the output of LDV is often used as a quality control of the measured velocity function, which is defined as

$$c(f) = \frac{\phi_{nv} \cdot \phi_{vn}}{\phi_{nn} \cdot \phi_{vv}} \tag{2}$$

in which ϕ_{nn} and ϕ_{vv} are the autospectra of $\tilde{N}(f_i)$ and $\tilde{V}(f_i)$, respectively. ϕ_{nv} and $\phi_{vn}$are cross-spectra between [$\tilde{N}(f_i)$ and $\tilde{V}(f_i)$] and [$\tilde{V}(f_i)$ and $\tilde{N}(f_i)$], respectively. The coherence function is a real-valued frequency function with values not greater than 1.0. Higher coherence function values correspond to better-measured velocity functions $\tilde{V}(f_i)$. Fig. 4(b) shows individual coherence functions associated with the magnitude of the velocity function in Fig. 4(a). On the target [at the grid point A and B marked in Fig. 3(a)], the surface velocity is highly amplified, resulting in high SNR. Therefore, the corresponding coherence functions approximate 1.0 almost throughout the entire frequency range.

To form a color (grayscale) map, the data in color (grayscale) dots in Fig. 3(a) are interpolated using nearest- neighbor interpolation and spatially filtered using two-dimensional (2-D) median filtering to achieve higher pixel resolution [10]. In this way, a color map derived from Fig. 3(a) is given in Fig. 3(b). Its 3-D representation is shown in Fig. 3(c). In Fig. 3, a "spot" of interest can be seen in all presentations, indicating presence of a mine. The size of the mine can be estimated by counting grid points [in Fig. 3(a)] across the spot. When a spot of interest is thought to indicate a mine, the middle of the spot is assumed to be associated with the center position of the buried mine. The laser beam can then be moved to that spot thereby marking the location on the ground. It usually points to the center of the mine with a radial accuracy of about two centimeters. The smaller the grid size (pixel), the higher the accuracy will be.

In similar fashion, Fig. 5 illustrates scanning results on a metallic M21 anti-tank mine buried 7.5 cm deep at U.S. Army Test Lane 11. The M21 mine is a cylinder with a top-view diameter of 22 cm. The individual magnitude velocity functions at scanning point A, B, C, and D as marked in Fig. 5(a) along with coherence functions are given in Fig. 6.

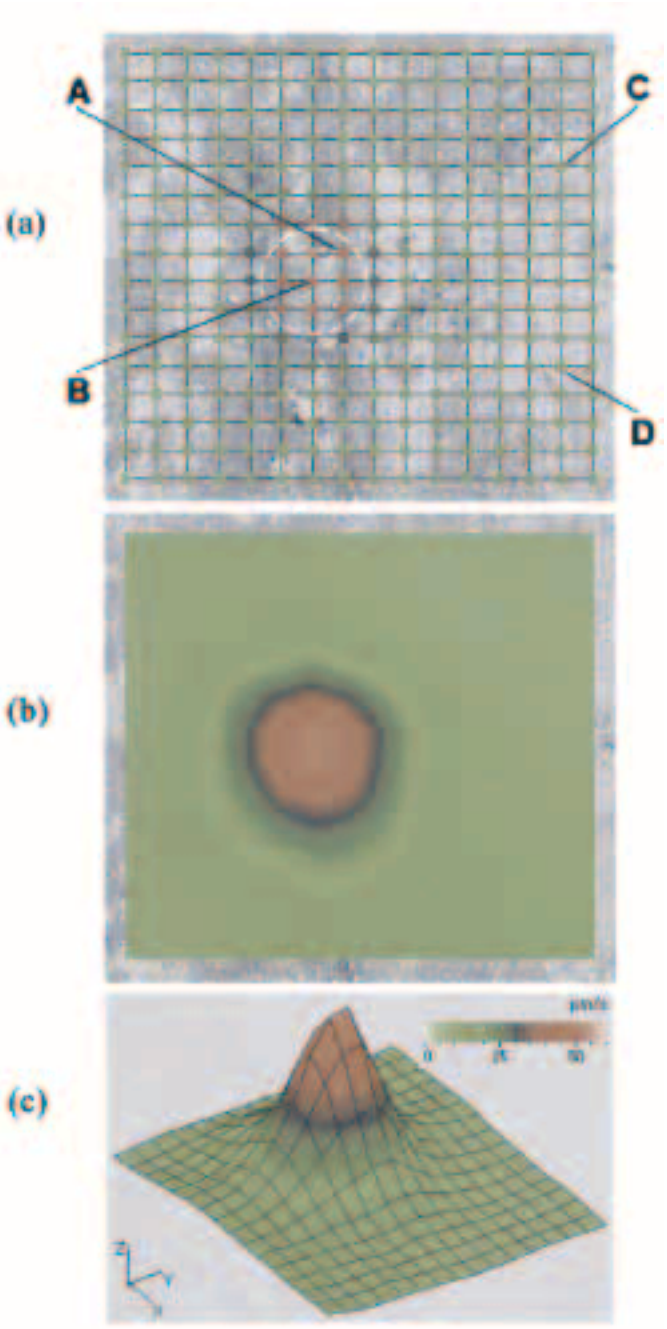

Fig. 5. A grid of 16 $\times$ 16 is defined covering a scanned patch of 1 m $\times$ 1 m resulting in a spatial resolution of 6.7 cm. It is superimposed on the image of the road surface at U.S. Army Test Lane 11. An M21 metallic mine is buried at 7.5 cm deep. The integrated (RMS) velocity value in a frequency band between 130 Hz and 160 Hz is represented. (a) Color dots. The dot-line circle indicates the target location. Color scale is given in (c). In Fig. 6, individual measured magnitude spectra on points A, B, C, and D are illustrated. (b) Color map, achieved from (a) in terms of interpolation and spatial filtering. Color scale is given in (c). (c) Three-dimensional (3-D) color map derived from (b).

Road types (depending on construction material), deep ground layering, and weathering conditions influence off-target velocity responses of the ground, hereafter referred to as background velocity responses. For example, Fig. 4(a) and Fig. 6(a) show that the background velocity lies below 13 μm/s in a relatively broad frequency band (from 100 Hz to 260 Hz) at the given acoustic excitation level. Mine types, burial depth, and

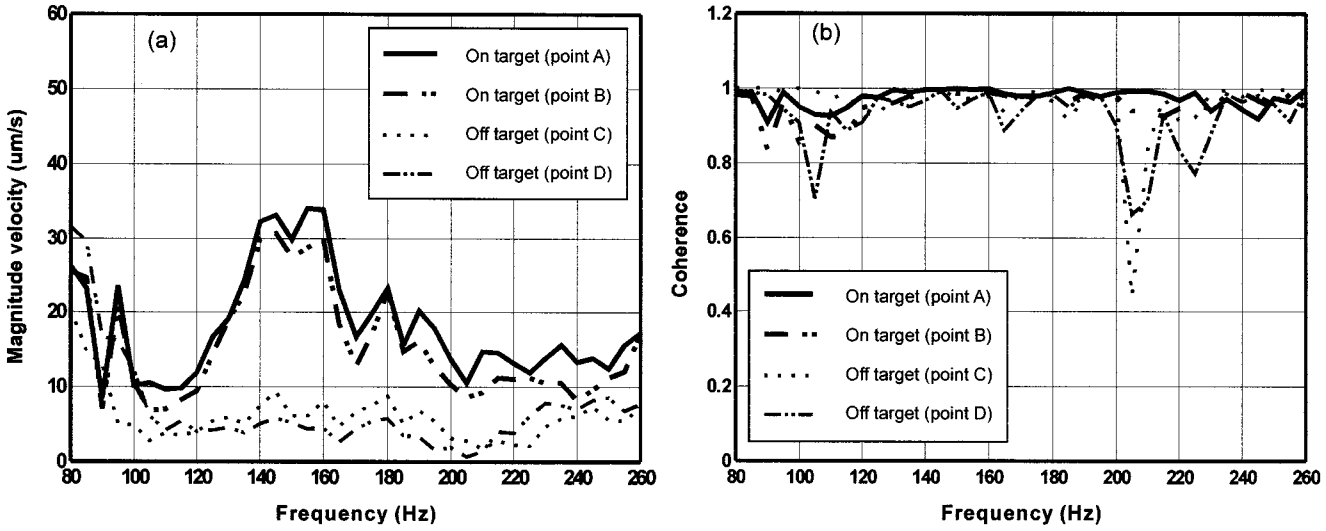

Fig. 6. Measured data on a metallic M21 antitank mine presented as functions of frequency at point A, B, C, and D marked in Fig. 5. (a) Magnitude spectra and (b) coherence functions.

road types predominate in determining signatures of on-target velocity. The detection ability is not significantly influenced by whether or not the mines are metallic or nonmetallic as shown in Figs. 3–6. The maximum ratio between on- and off-target velocity in a suitable frequency band can range from tens down to two.

Since detection of mines depends upon determining the difference between the ground velocity over a mine and away from a mine (or the background), it is important to study the variability of background velocity functions measured using the current LDV system. Taking a sandy-gravel road in U.S. Army Test Lane 13 as an example (as shown in Fig. 7), background velocity functions, both within a 1 m^2 patch and throughout a 20-m length of road, have reasonably low variability in the frequency range between 120 Hz and 200 Hz at a given acoustic excitation level. They also assume low values within this range.

Often deeper and/or smaller mines lead to scanning results with a lower on-/off-target ratio. In such circumstances, the decision concerning the presence of a mine becomes more difficult due to clutter. Exploiting the broadband nature of mine signatures facilitates ruling out anomalies and clutter since they result in narrow-band responses relative to the mine signature. Therefore, narrow band analysis is performed along a relatively broad frequency band within which consistent amplifications caused by buried mines are expected. Fig. 8 shows an example typical of a deeply buried mine resulting in a low on-/off-target ratio. A circular spot in the color maps remains relatively stable when stepping a 20-Hz-wide subband through a frequency band between 110 Hz and 180 Hz. In this overall broadband, the mine caused consistent amplification in the magnitude of velocity. In this example, the 20-Hz-wide subband is overlapped at 10 Hz when stepping through the overall broad band.

Note that in the lower-right corner of each color map, a small spot was caused by an inhomogenity of the sound field throughout the entire patch. The sound waves propagate from the lower-right to the upper-left corner in the color maps shown in Fig. 8. The sound source was located 1.8 m away from the center of the scanned patch. For the frequency band used, the scanned patch can be considered within the near field. It is obvious that when a mine is located closer to the lower-right corner of the color maps shown in Fig. 8, a decision on presence of a mine would become more difficult. For this reason, it is very important to be able to animate the scanning results. Using animation, a wave front of the acoustic excitation can be shown traveling from the lower-left to the upper right corner in this example. A mine "spot" vibrates at the same location up and down. In animating the scanned results, both magnitude and phase information of the surface velocity are exploited.

At a specific frequency f_0, the complex velocity function $\tilde{V}_{ij}(f)$ is used to achieve instantaneous values

$$I_{ij}(t) = \left|\tilde{V}_{ij}(f_0)\right| \cos\left[\frac{2\pi}{T_A}t + \varphi_{ij}(f_0)\right] \tag{3}$$

where $\varphi_{ij}(f)$ is the phase function of $\tilde{V}_{ij}(f)$ taking the phase function of acoustic excitation into account. T_A is the time period introduced artificially for the purpose of animation. With increasing time t, instantaneous values $I_{ij}(t)$ throughout the entire grid can be visualized in the form of a periodic animation, a powerful tool for distinguishing buried mines from clutter.

In general, three factors primarily influence the decision concerning whether or not a mine is present. The magnitude of velocity is used as the first major cue to detect mines. With consistent amplification of the magnitude of velocity over a relative broad frequency band, the next major cue is a circular shape in the scanning image that remains almost unchanged when stepping through the overall frequency range with a subband. Clutter enters and exits from the subband image. Lastly, the size of the spot of interest is exploited for a decision. Occasionally, the phase information is also used in terms of animating scanning images to enhance identification of the circular-shaped target and to suppress anomalies.

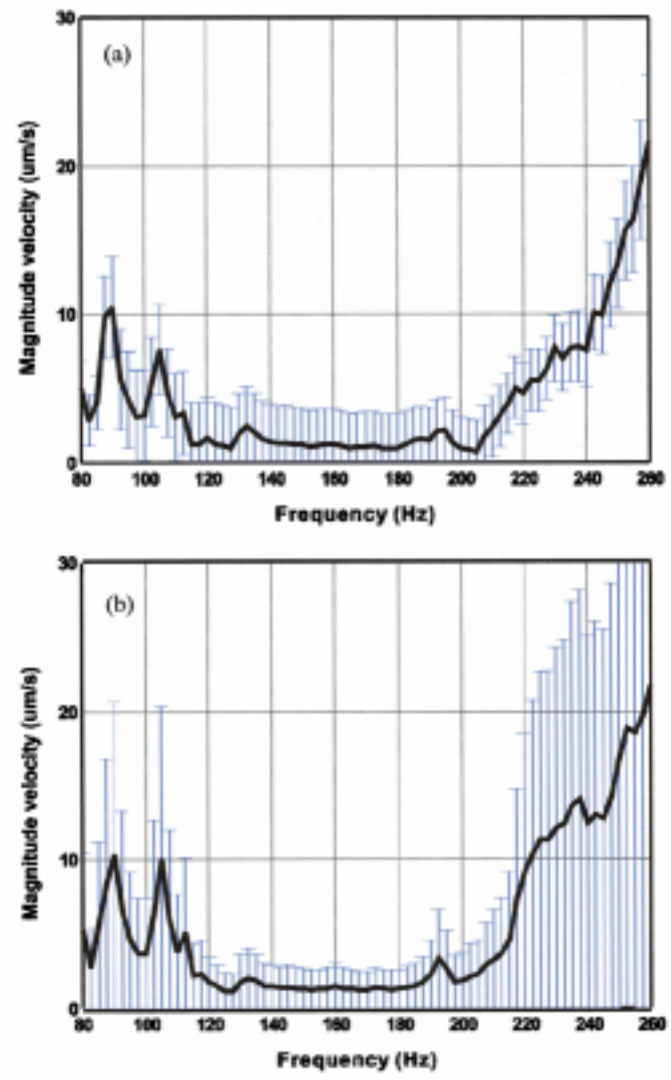

Fig. 7. Variability of background velocity functions in a sandy gravel road, measured using the LDV-based A/S mine detection system. The standard deviation of the overall background velocity is presented as error bars across the average values for each frequency. Averaged background velocity functions are achieved in terms of averaging all magnitude velocity functions expect for those on a target. (a) Averaged background velocity function evaluated within 1 m^2. (b) Averaged background velocity function from eight 1 m^2 patches throughout the sandy-gravel road of 20 m long.

IV. Blind Testing at Fort A. P. Hill

To demonstrate the capability of a detector in a scenario as nearly approximating real minefields as possible, testing must be conducted without the testers knowing whether or not a mine is present. These tests are referred to as "blind" tests. During April 1999, the University of Mississippi participated in an army-sponsored blind test using the laser Doppler vibrometer-based A/S coupling landmine detection system. Throughout the blind test, the A/S coupling-based landmine detection apparatus was set up as shown in Fig. 2. As a sound source, two loud speakers were placed at a distance 1.8 m from the center of a patch to be scanned. The sound source radiated pseudo-random noise covering the frequency range between 80 and 300 Hz. The LDV was mounted onto a vehicle-based platform at a height 3.5 m from the ground surface and the laser beam of the LDV was focused downward onto the ground surface.

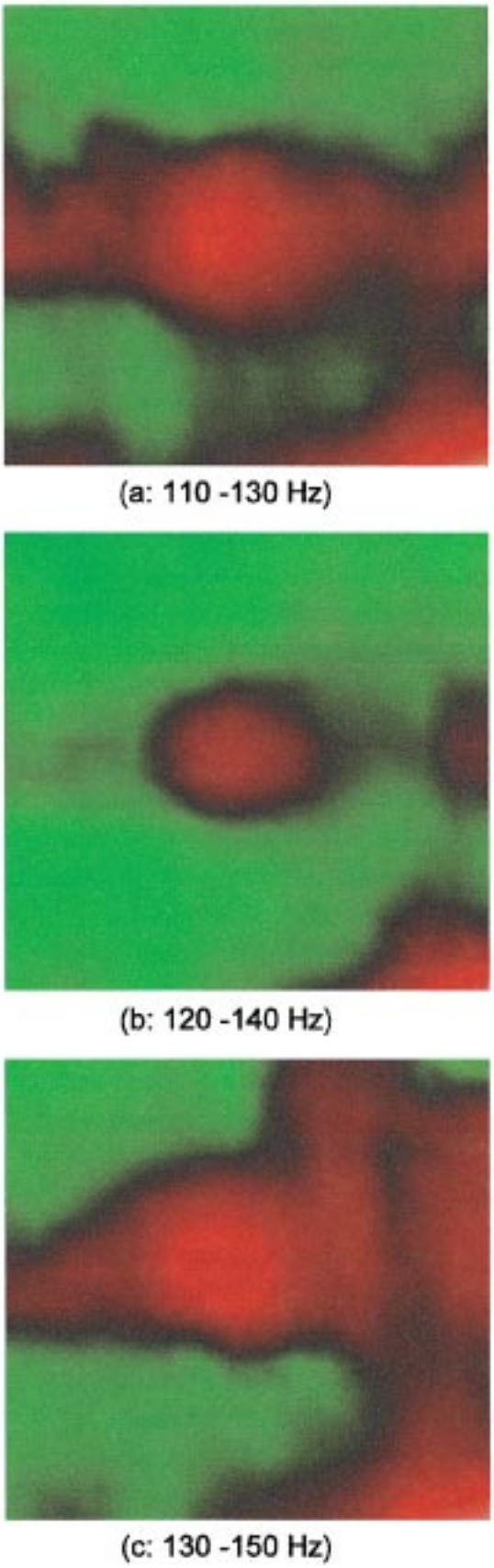

Fig. 8. Narrowband analysis of scanning results achieved from a deeply buried mine in a sandy-gravel road. When stepping a 20-Hz-wide subband through a frequency range between 110 Hz and 150 Hz, a circular spot remains relatively stable at the same position while other anomalies and clutter change their position and shape. Some of them come and go. When stepping through the entire band, it is reasonable to overlap the subband slightly.

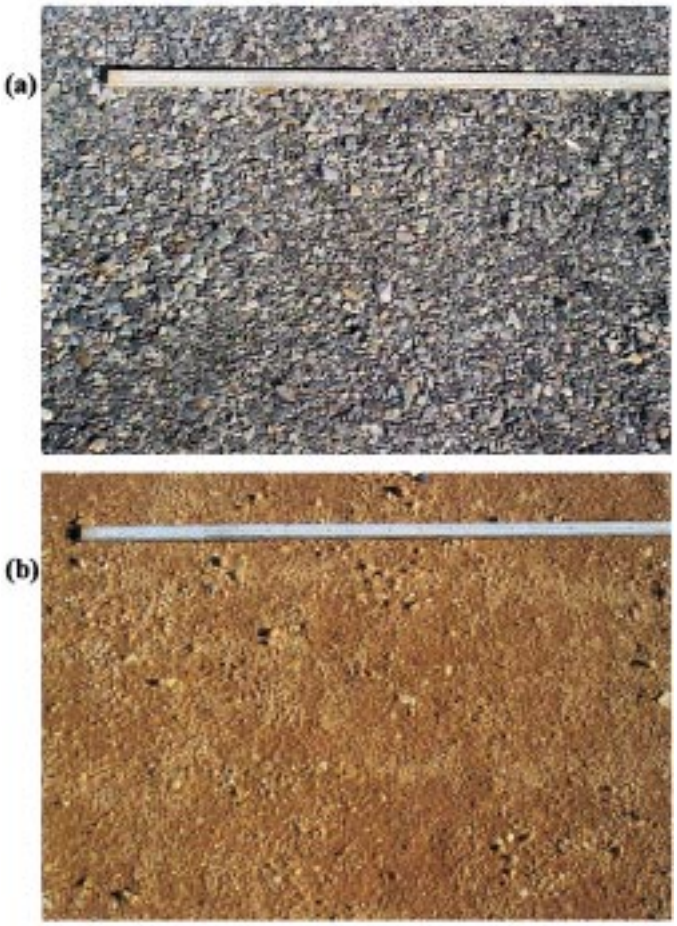

Fig. 9. Photographs of two different road surfaces in the blind test lanes. P. Hill. (a) Ground surface of a gravel road. (b) Ground surface of a sandy-gravel road.

The test area consisted of 59 predetermined 1 m $\times$1 m patches in two different road types. Fig. 9 shows photographs of these two road surfaces. Prior to the blind test, it was known that the location of the center of a mine did not necessarily coincide with the center of the square scanned patch if a mine was present. After finishing the blind test, the scorer revealed that 19 of the scanned patches contained antitank mines buried between one and six inches deep. Table I lists the distribution of different depths among the 19 mines. 31 of the remaining scanned patches were randomly-chosen blank patches which did not contain mines. The remaining nine patches were chosen due to a high correlation with ground penetrating radar (GPR) clutter from previous GPR tests.

To ensure covering the majority of the diameters of buried mines within the scanned area, the patches were scanned using a larger area of 1.5 m $\times$ 1.5 m. To speed up scanning, three types of scans and a set of rules to govern use of these scans were defined in the scanning strategy. At each scanned patch, the first scan used 16 $\times$ 16 grid points, resulting in a 10-cm spatial resolution, and used a 10 Hz frequency resolution over the frequency range between 80 and 300 Hz. The complex velocity function at each grid point was averaged over three scanning periods. This first *coarse* scan took approximately 3–4 min and was usually sufficient for detecting mines when they were

TABLE I
DISTRIBUTION OF ANTITANK MINES IN DIFFERNET DEPTHS IN A RECENT BLIND TEST AT FORT A. P. HILL (1 IN = 2.54 CM)

Depth (inches)	*Number of mines*
1	6
2	6
3	3
4	1
6	3

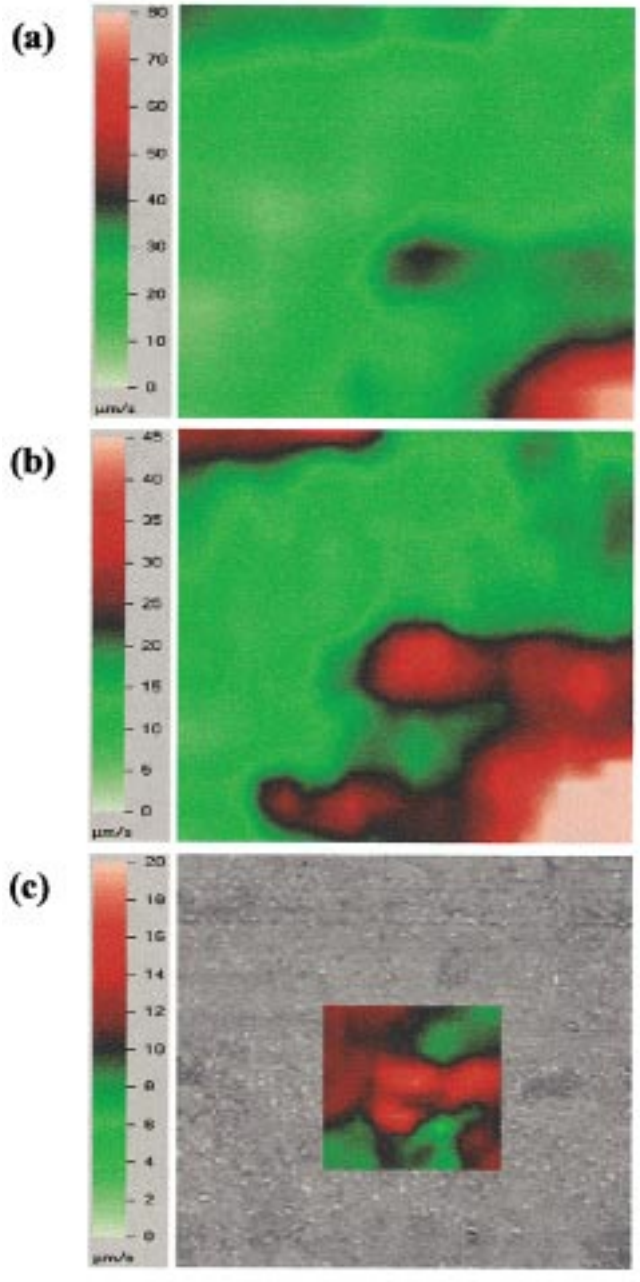

Fig. 10. Scan results on one patch in the blind test lanes. (a) Coarse scan: 16 $\times$ 16 grid points covering an area of 1.5 m $\times$ 1.5 m. (b) Fine scan: 22 $\times$ 22 grid points covering an area of 1.5 m $\times$ 1.5 m. A spot of interest near the center was identified (c) Zoom scan: 16 $\times$ 16 grid points covering an area of 0.5 m $\times$ 0.5 m containing the spot of interest identified by the fine scan. The spot of interest is resolved into three small pieces after the zoom scan leading to the decision: "no mine."

TABLE II
RESULTS OF THE BLIND TEST FOR DETECTION OF ANTITANK MINES

	Probability of detection	*False alarm rate (m^{-2})*	*Coarse detections*	*Fine detections*	*Zoom detections*
Gravel road	9/10 = 90%	0/15 = 0.00	8	1	0
Sandy-gravel road	9/9 = 100%	1/16 = 0.06	6	2	1
Overall	18/19 = 95%	1/31 = 0.03	14	3	1
Clutter		0/9 = 0.00			

not buried deeper than 4 in. A *fine* scan consisted of 22 × 22 grid points corresponding to a 7 cm spatial resolution and used a frequency resolution of 5 Hz. Five complex averages were performed to achieve one period of velocity function at each grid point. Including more scan points, using a higher frequency resolution and increasing the number of averages led to this *fine* scan lasting approximately 22 min. For finer resolution to identify areas of interest, a zoom scan was then performed. The *zoom* scan contained 16 × 16 grid points, covering an area of 0.5 m × 0.5 m, resulting in a 3 cm spatial resolution and used a frequency resolution of 5 Hz. Zoom scans took approximately 8 min to complete. The fine scan was only needed a few times and most resulted in a declaration of "no mine." There were fewer zoom scans and only one led to a decision that a mine was present.

As an example, Fig. 10 illustrates the scanning results on one scanned patch from the blind test in which all three scan types had to be applied step-by-step. The coarse scan results in the form of a color map are shown in Fig. 10(a). Since the center of a mine had to be within the area of 1 m × 1 m, a spot of high magnitude velocity on the lower-right corner was considered to not be of interest. A spot near the center of the scanned area became clearer when defining the color scale representing the velocity range between 0 and 45 μm/s. A fine scan was then performed by increasing the spatial and frequency resolutions and the number of averages. The color map of the fine scan as shown in Fig. 10(b) confirmed the spot of interest near the center of the scanned area. Its size may have been suitable for a potential mine. Its shape, however, had to be resolved with more detail before a final decision could be made. For this reason, a zoom scan was used by defining a smaller area including only the spot of interest, thus increasing the spatial resolution to 3 cm by using 16 × 16 grid points covering an area of 0.5 m × 0.5 m. The spot of interest was then resolved into three small pieces as shown in Fig. 8(c), leading to a decision that no mine was present.

The results of the blind test as provided by the Institute of Defense Analysis (IDA) are summarized in Table II (see also [11]). Probability of detection and false alarm rates were reported for each of the test lane road types and for the combined lanes. False alarm rates were computed as the number of scans in which the results indicated the presence of a mine when there was no mine divided by the number of blank sites scanned. No false alarms were declared in any of the nine of the GPR clutter patches. Of the 18 total detections, 14 were made without the use of either the fine or the zoom scans. The one mine that was undetected in the gravel road lane was buried at a depth of 6 in. When a scan result revealed the presence of a mine, the laser beam of the LDV was brought to the center of the circular spot marking the ground. The accuracy of mean radial distance of the marked center from the actual center of the mines according to the ground truth survey for all detections was approximately 5 cm. Thus, the marked center fell within the footprint of the mine in each instance.

V. CONCLUSIONS

Knowledge of the physics of A/S coupling is of central importance to understanding the propagation mechanism of acoustic energy-induced waves in the subsurface under the ground. The porous nature of the ground permits land mine detection based upon the distinct changes of the A/S coupled motion on the ground surface when a target is buried beneath the surface. Because this methodology senses changes of the A/S coupled motion in the ground, both metallic and nonmetallic mines can be detected. This led to the development of a novel sensor for landmine detection technology: the laser-Doppler vibrometer-based acoustic landmine detection system.

The current acoustic landmine detection system utilizes a scanning single-beam laser Doppler vibrometer for sensing the A/S coupled motion on the ground surface. Complex surface velocity functions of frequency are measured using a remote, raster-scanning technique.

In general, three factors are used to detect antitank mines: magnitude of the velocity function and the shape and size of the area with increased velocity. The scanning results are transformed into an image form. Mine signatures are found to be broadband in nature. A mine is determined to be present when there is consistent amplification of the magnitude velocity over a relatively broad frequency band and when a circular shape in the scanning image remains almost unchanged when stepping through the overall frequency range with a subband. Clutter enters and exits the image as the subbands are changed. In addition to the circular shape, the size of the spot of interest is exploited for a decision. Occasionally, the phase information is also used in terms of animating scanning images to enhance identification of circular-shaped targets and to suppress anomalies.

Applying all the analysis tools described in this paper, the scanning laser Doppler vibrometer-based A/S mine detection system achieved a probability of detection of 95% with a false alarm rate of 0.03 m^2 in a recent field blind test. Up to the current time, the research effort has been dedicated to demonstrating the feasibility in field measurements using the acoustic technology for landmine detection rather than achieving a high scanning speed. Field tests have been conducted on a limited number of road types. Therefore, the results described in the current work are restricted to those burial conditions. The detection ability of the current system in other field conditions, such as on frozen ground and water- saturated ground, is the subject of further investigation.

In the next research and development phase, efforts will be made to develop the current technique into a vehicle-mounted field device. To facilitate this, research is being conducted to speed up the scanning procedure [12], [13], improve the measurement performance [14], and automatically recognize targets [11].

ACKNOWLEDGMENT

The authors would like to thank Dr. T. Witten and E. Rosen for their assistance in this effort. The authors would also like to

thank R. Craig for his dedication and expertise in collecting the data for this paper.

REFERENCES

[1] H. E. Bass, L. N. Bolen, D. Cress, J. Lundien, and M. Flohr, "Coupling of airborne sound into the earth: Frequency dependence," *J. Acoust. Soc. Amer.*, vol. 67, pp. 1502–1506, 1980.

[2] J. M. Sabatier, H. E. Bass, L. N. Bolen, and K. Attenborough, "Acoustically deduced seismic waves," *J. Acoust. Soc. Amer.*, vol. 80, pp. 646–649, 1986.

[3] M. A. Biot, "Theory of propagation of elastic waves in a fluid-saturated porous solid. II: Higher frequency range," *J. Acoust. Soc. Amer.*, vol. 28, pp. 179–191, 1956.

[4] J. M. Sabatier, H. E. Bass, L. N. Bolen, K. Attenborough, and V. V. S. S. Sastry, "The interaction of airborne sound with the porous ground. The theoretical formulation," *J. Acoust. Soc. Amer.*, vol. 79, pp. 1345–1352, 1986.

[5] C. J. Hickey and J. M. Sabatier, "Measurements of two types of dilatational waves in an air-filled unconsolidated sand," *J. Acoust. Soc. Amer.*, vol. 102, pp. 128–136, 1997.

[6] N. Xiang and J. M. Sabatier, "Land mine detection measurements using acoustic-to-seismic coupling," in *Proc. SPIE*, A. C. Dubey, Ed., Orlando, FL, 2000, pp. 645–655.

[7] W. P. Arnott and J. M. Sabatier, "Laser-Doppler vibrometer measurements of acoustic to seismic coupling," *Appl. Acoust.*, vol. 30, pp. 279–291, 1990.

[8] J. M. Sabatier and N. Xiang, "Laser-Doppler based acoustic-to-seismic detection of buried mines," in *Proc. SPIE*, A. C. Dubey, Ed., Orlando, FL, 1999, pp. 215–222.

[9] C. B. Scruby and L. E. Drain, *Laser Ultrasonics Techniques and Applications*. Bristol/Philadelphia/New York: Adam Hilger, 1990.

[10] *Matlab user's Guide: Image Processing Toolbox*: The Math Works Inc..

[11] E. M. Rosen, K. D. Sherbondy, and J. M. Sabatier, "Performance assessment of a blind test using the university of Mississippi's acoustic/seismic laser Doppler vibrometer (LDV) mine detection apparatus at A. P. Hill," in *Proc. SPIE Conf. Detection and Remediation Technologies for Mines and Minelike Targets V*, A. C. Dubey, Ed. Orlando, FL, 2000, pp. 656–666.

[12] N. Xiang and J. M. Sabatier, "Fast M-sequence transform for laser-Doppler based mine detection," in *Proc. SPIE Conf. Signal Processing, Sensor Fusion, and Target Recognition VIII*, I. Kadar, Ed. Orlando, FL, 1999, vol. SPIE 2720, pp. 390–396.

[13] D. Costley, V. Valeau, and N. Xiang, "Continuous scanning laser Doppler vibrometer for mine detection," in *Proc. SPIE Conf. Detection and Remediation Technologies for Mines and Minelike Targets V*, A. C. Dubey, Ed. Orlando, FL, 2000, pp. 711–718.

[14] P. Goggans, C. R. Smith, and N. Xiang, "Increasing speckle noise immunity in LDV-based acoustic mine detection," in *Proc. SPIE Conf. Detection and Remediation Technologies for Mines and Minelike Targets V*, A. C. Dubey, Ed. Orlando, FL, 2000, pp. 719–724.

James M. Sabatier received the Ph.D. degree from the University of Mississippi, University, in 1984.

He is currently a Senior Research Scientist with the University of Mississippi's National Center for Physical Acoustics and an Associate Professor of Physics and Astronomy. His research focuses primarily on acoustic phenomena in porous materials.

Ning Xiang received the Ph.D. degree in electrical and electronic engineering from Ruhr-University of Bochum, Bochum, Germany, in 1990. He worked as a Project Manager for Head Acoustics, Inc., Germany, from 1991 to 1996, and joined Fraunhofer-Institut, Germany, as a Research Scientist in 1997.

Since 1998, he has been a Research Scientist with the National Center for Physical Acoustics and an Adjunct Associate Professor of Electrical Engineering with the University of Mississippi, University.

Dr. Xiang is a member of the Acoustical Society of America and the Acoustical Society of Germany.